Lost surface waves in nonpiezoelectric solids

Eugene A. Eliseev, Anna N. Morozovska, Maya D. Glinchuk, and Sergei V. Kalinin

Phys. Rev. B **96**, 045411 — Published 11 July 2017

DOI: 10.1103/PhysRevB.96.045411

Submitted to PRB, revised version

Lost surface waves in non-piezoelectric solids

Eugene A. Eliseev,[1] *Anna N. Morozovska,*[2,3*] *Maya D. Glinchuk*[1]*, and Sergei V. Kalinin*[4, †]

[1]Institute for Problems of Materials Science, National Academy of Sciences of Ukraine,
3, Krjijanovskogo, 03142 Kyiv, Ukraine
[2]Institute of Physics, National Academy of Sciences of Ukraine,
46, Prospekt Nauky, 03028 Kyiv, Ukraine
[3]Bogolyubov Institute for Theoretical Physics, National Academy of Sciences of Ukraine,
14-b Metrolohichna str. 03680Kyiv, Ukraine
[4]Center for Nanophase Materials Science, Oak Ridge National Laboratory, Oak Ridge, Tennessee 37831, USA

Abstract

The existence of shear surface acoustic waves (SAWs) was regarded impossible in non-piezoelectrics with homogeneous flat surfaces. We showed that transverse shear SAWs can propagate near the flat surfaces of all crystalline dielectrics due to the omnipresent flexoelectric coupling. It appeared that the penetration depth of the previously unexplored SAW is defined by the flexocoupling strength. Since the SAW occurs due to the flexoelectric coupling, we named it flexoelectric SAW (Flexo-SAW). We predict that the phonon spectra corresponding to the Flexo-SAWs and bulk phonon modes can be separated in thin non-piezoelectric films, such as strontium titanate.

[*] Corresponding author. E-mail: anna.n.morozovska@gmail.com (A.N.M.)

[†] Corresponding author. E-mail: sergei2@ornl.gov (S.V.K.)

I. INTRODUCTION

A. Amazing dynamics at the surfaces of solids. The physical processes taking place at the surface of solids are so versatile that becomes an inexhaustible subject of fundamental research [1, 2]. In particular, since the discovery of surface waves in solids [3], they focus the increasing attention of scientists [4, 5], because their experimental and theoretical studies can serve as the source of unique information about the surface impact on the dynamics and structure of atomic lattice [6], structural instabilities and phase transitions induced by the surface [7], and explore the properties of phonons in spatially confined systems [8, 9]. In addition to the fundamental aspect, the surface oscillations and waves are indispensable for applications in modern nanoacoustics [10] and nanoplasmonics [11].

B. Surface waves: from the discovery to nowadays. Existence of the surface acoustic waves (**SAWs**) in solids of arbitrary symmetry (including the isotropic one) had been predicted at the end of the 19th century by Lord Rayleigh [3]. The main conclusion made from the Rayleigh solution is that the shear surface wave cannot propagate along the flat surface. The longitudinal-transverse Rayleigh waves are the mixture of shear and dilatation waves of expansions and compressions, in contrast to the acoustic waves propagating in the bulk of a solid matter, which have two transverse shear modes and a longitudinal dilatational one [12]. Only at the end of the sixties of the 20th century Bleustein [13] and Gulyaev [14] had shown that purely shear surface waves can propagate in some solids without inversion center (e.g., at definite crystallographic cuts of piezoelectrics), and naturally their appearance is impossible in all non-piezoelectrics with a homogeneous flat surface. Nonlinear Rayleigh waves propagating along the flat surface of a homogeneous solid medium covered by a thin film were considered in 1998 by Eckl et al [15]. The influence of a standing SAWs on the diffusion of an adatom was theoretically studied in 2011 by Taillan et al [16]. Recently the interest to the theoretical consideration of classical linear SAWs was renewed by Romero [17], who considered several types of SAWs in piezoelectrics with an ideal flat surface.

Notably, if the surface is not flat the shear waves can appear. In particular, Auld and Gagnepain [18] revealed that any periodic corrugation of the surface (including a very shallow one) leads to shear surface waves. Furthermore, Love waves [12, 19] are shear surface waves of a planar substrate coated with a thin layer. The appearance of shear surface waves for a planar substrate supporting an array of mechanical resonators has been reported [20]. Hence one can readily imagine the situation that the observation of shear SAWs at the surface of a non-piezoelectric will be attributed to surface corrugation [18], artificial inhomogeneities [20] or additional layers [19]. However, in the latter case, SAWs are possible only for a certain ratio between the elastic modules of the layer and the substrate [19]. The conditions for the existence of shear SAWs on corrugated surfaces essentially depend on the form of the inhomogeneity [18]; they are far from being

omnipresent. Running ahead, the aim of this work is to show that for the flat surface of an arbitrary solid body (including an isotropic one in the sense of elastic properties) the localization of transverse acoustic waves is always possible under the influence of the omnipresent flexoelectric effect, including the case when all previous theories predicted the complete absence of transverse SAWs.

C. Experimental observations of SAWs. The questions how to investigate experimentally SAWs and how to verify existing theoretical predictions [13-17] along with many others naturally arise. Since the frequency of the soft mode related optic and acoustic phonons in piezoelectric and paraelectric ferroics typically lays within THz region and corresponding wave vectors are in the range (0.05 – 5)nm^{-1}, the phonon spectra $\omega(k)$ can be extracted from the inelastic neutron scattering experiments [21, 22, 23, 24, 25, 26] by a conventional procedure. Namely each experimental point of the spectra $\omega_i(k_i)$ (e.g., shown in fig.2 in Ref.[21]) is defined from the energy position $\hbar\omega_i$ of inelastic neutron scattering intensity peak measured at fixed wave vector k_i (see, e.g., fig.1 in Ref. [21]).

Hamilton et al. [27] performed the first experiment demonstration that SAW in quartz can be probed by diffraction of cold neutrons. Much earlier Soffer et al [28] proposed an optical imaging method for direct observation and study of SAWs at the nonpolar Y-cut of piezoelectric $LiNbO_3$ (typical manifestation of Bleustein and Gulyaev waves). Pyrak-Nolte et al. [29] made the first direct observation of the new class of elastic interface waves propagating along the discontinuity of a synthetic fracture in aluminum. De Lima Jr et al. [30] presented the experimental observation of Bloch oscillations, the Wannier-Stark ladder, and Landau-Zener tunneling of SAW in perturbed grating structures on a solid substrate (at that the vertical surface displacement has been measured by interferometric methods).

Fine aspects of the SAWs can be explored by Brillouin [11, 31, 32] and Raman [33, 34] scattering, ultrasonic pulse-echo method [31, 32] allowing hypersound spectroscopic measurements, and Surface Enhanced Raman scattering based on the incomplete internal reflection [35]. Also there are many advanced techniques for SAWs observations operating in GHz range of frequencies, such as laser ultrasonics experiments [36], optical interferometry [37] and surface Brillouin light scattering [38, 39]. These methods are mostly relevant for SAWs observations up to (10 – 100) GHz range, however they unlikely can "see" SAWs in THz range of frequencies that is typical for proper and incipient inorganic ferroelectrics.

Thus (except for the THz region) the experimental methods of SAW observation are well-evolved and enough precise to probe their finest properties and to verify the most sophisticated theoretical predictions.

D. Expected role of the flexocoupling on the surface waves. It should be noted that static flexoelectric effect [40, 41, 42, 43], consisting in the appearance of polarization due to the strain gradient (direct flexoeffect), and the appearance of strain due to the polarization gradient (converse flexoeffect), was not taken into account in all known theories of SAWs [3, 12 – 17]. The strain induced by the flexoelectric coupling is linearly proportional to the polarization gradient, $u_{ij}^{sf} = -f_{ijkl}\left(\partial P_k / \partial x_l\right)$, here f_{ijkl} are the components of flexocoupling tensor [40 – 45], P_k are polarization components. The static flexoelectric effect exists in all solids, as allowed by arbitrary symmetry, and its strength can be small, moderate or giant, because f_{ijkl} ranges from (0.1 – 1) volts [41-45] to hundreds of volts [44].

Moreover the notion about dynamic flexoelectric effect [43, 45, 46], consisting in the appearance of polarization P_i^{df} in response to accelerated motion of the medium in the time domain, and its impact on phonon spectra has been absent until recently [47, 48]. The dynamic flexoelectric effect was firstly introduced by Tagantsev [43, 49] as $P_i^{df} = -M_{ij}\left(\partial^2 U_j / \partial t^2\right)$, where U_j is an elastic displacement and M_{ij} is a flexodynamic tensor.

Nevertheless, an elastic wave of any kind is inevitably accompanied by a periodic gradient of mechanical strain and stress. This gradient is proportional to the wave vector of the oscillation and is obviously small for longer wavelengths. For a media of arbitrary symmetry (including an isotropic one) the wave of the strain gradient will cause a wave excitation of electric polarization (i.e., the local polarization, the mean value of which is zero) due to the direct flexoelectric effect. The latter, in turn, will affect the elastic stresses associated with the wave due to the converse flexoelectric effect. Thus the flexocoupling should influence the properties of surface waves in all solids, since it essentially affects the bulk phonon spectra in different ferroelectrics and paraelectrics [46 - 49], and the influence should be more pronounced for shorter wavelengths.

E. Research motivation, impact and methods. Recently using Landau-Ginzburg-Devonshire (**LGD**) phenomenological continuum media approach Morozovska et al. [47, 48] demonstrated the significant influence of the flexocoupling on the appearance of spatially modulated phases and on the properties optic and acoustic phonons in the ferroelectric and paraelectric phases of ferroelectrics $PbTiO_3$, $Sn_2P_2(S,Se)_6$, and paraelectric $SrTiO_3$. Motivated by these results we used LGD approach for SAWs description in paraelectrics. We revealed that the surface shear waves similar to the waves of Bleustein [13] and Gulyaev [14] can exist in dielectrics of any symmetry (e.g. in paraelectric $SrTiO_3$) and for an arbitrary orientation of the surface due to the flexoelectric coupling. The wave is the oscillation of shear strain coupled with electric polarization. Below we classify ~~the~~ this type of waves as **flexocoupling-induced SAWs** (briefly as **Flexo-SAWs**).

Note that previously known types of SAWs (see e.g. Refs.[12-19]) have been revealed within phenomenological continuum media approach. We emphasize that our choice of the phenomenological LGD approach conditions the generality of the obtained results, and it shows that the predicted Flexo-SAWs exist for all non-piezoelectric solids, whereas microscopic *ab-initio* approaches are material specific.

II. STATEMENT OF THE PROBLEM ALLOWING FOR THE FLEXOCOUPLING

LGD expansion of bulk (F_V) and surface (F_S) parts of Helmholtz free energy F on the polarization vector (P_i) and strain tensor components (u_{ij}) has the form [47-48]:

$$F_V = \int_V d^3r \begin{pmatrix} \frac{a_{ij}}{2} P_i P_j + \frac{a_{ijkl}}{4} P_i P_j P_k P_l - P_i E_i + \frac{g_{ijkl}}{2}\left(\frac{\partial P_i}{\partial x_j}\frac{\partial P_k}{\partial x_l}\right) - q_{ijkl} u_{ij} P_k P_l \\ -\frac{f_{ijkl}}{2}\left(P_k \frac{\partial u_{ij}}{\partial x_l} - u_{ij}\frac{\partial P_k}{\partial x_l}\right) + \frac{c_{ijkl}}{2} u_{ij} u_{kl} + \frac{v_{ijklmn}}{2}\left(\frac{\partial u_{ij}}{\partial x_m}\frac{\partial u_{kl}}{\partial x_n}\right) \end{pmatrix}, \quad (1a)$$

$$F_S = \int_S d^2r \frac{a_{ij}^S}{2} P_i P_j \ . \quad (1b)$$

The components of tensor a_{ij} are positively defined constants for linear dielectric and explicitly depend on temperature T for ferroelectrics and paraelectrics. In particular, a Barrett-type [50] formula $a_{ij} = \alpha_{ij}^T\left(T_q \coth\left(T_q/T\right) - T_C\right)$ is valid for incipient paraelectrics like $SrTiO_3$, wherein α_{ij}^T are the inverse Curie-Weiss constants, T_C is the Curie temperature, T_q is a characteristic temperature. All other tensors in the free energy (1) are supposed to be temperature independent. Tensor a_{ijkl} should be positively defined for the functional stability in paraelectrics and ferroelectrics; it can be neglected for linear dielectrics. Tensors g_{ijkl} and v_{ijklmn}, which determine the magnitude of the gradient energy, are also regarded positively defined. Coefficients q_{ijkl} are the components of electrostriction tensor; c_{ijkl} are the components of elastic stiffness tensor. Polarization is conjugated with electric field E_i that can include external and depolarization contributions (if any exists). The flexoelectric energy is written in the form of Lifshitz invariant, $\frac{f_{ijkl}}{2}\left(P_k \frac{\partial u_{ij}}{\partial x_l} - u_{ij}\frac{\partial P_k}{\partial x_l}\right)$, where f_{ijkl} is the flexocoupling stress tensor.

Lagrange function is

$$L = \int_t dt\left(F - K\right), \quad (2)$$

where the kinetic energy K is given by expression [43, 45, 47, 49],

$$K = \int_V d^3 r \left(\frac{\mu}{2} \left(\frac{\partial P_i}{\partial t} \right)^2 + M_{ij} \frac{\partial P_i}{\partial t} \frac{\partial U_j}{\partial t} + \frac{\rho}{2} \left(\frac{\partial P_i}{\partial t} \right)^2 \right), \tag{3}$$

that includes the dynamic flexoelectric coupling tensor M_{ij}. U_i is the elastic displacement and ρ is the density of a material. The strain components are related with the displacement derivatives in a conventional way, $u_{ij} = \frac{1}{2}\left(\frac{\partial U_i}{\partial x_j} + \frac{\partial U_j}{\partial x_i} \right)$.

Dynamic equations of state have the form of Euler-Lagrange (**E-L**) equations:

$$\frac{\delta L}{\delta P_i} = -\Gamma \frac{\partial P_i}{\partial t}, \qquad \frac{\delta L}{\delta U_i} = 0. \tag{4}$$

For most of the cases one can neglect the polarization relaxation by setting $\Gamma = 0$ and omit high order elastic strain gradient by setting $v_{ijklmn} = 0$, if the flexoelectric coefficients are below the critical values f_{ijkl}^{cr} [51, 52]. For the flexoelectric coefficients higher than the critical ones the spatially modulated phase occurs [48], at that the relationship $f_{ijqs}^{cr} f_{klqs}^{cr} \cong g_{ijmn} c_{klmn}$ is valid under the condition $v_{ijklmn} = 0$ [48, 51, 52].

Hereinafter we regard that the dynamic flexoeffect tensor is diagonal, $M_{ij} = M\delta_{ij}$, and the inequality $M^2 < \rho\mu$ should be valid for the stability of kinetic energy [see Eq.(3)]. Below we use an isotropic approximation for the tensor coefficients $a_{ij}^S = \alpha_{S0}\delta_{ij}$ and $a_{ij} = \alpha(T)\delta_{ij}$, where α_{S0} is the surface energy coefficient, $\alpha(T) = \alpha_T \left(T_q \coth\left(T_q / T \right) - T_C \right)$ and δ_{ij} is a Delta-Kroneker symbol.

The boundary conditions at mechanically free surface can be obtained from the variation of the free energy (1) on polarization and strain:

$$g_{kjim} n_k \frac{\partial P_m}{\partial x_j} + \alpha_{S0} P_i = -\frac{f_{jkim}}{2} u_{jk} n_m \Big|_S. \qquad \sigma_{ij} n_j \big|_S = 0. \tag{5}$$

Here n_k are the components of the external normal to the surface, elastic stress tensor $\sigma_{ij} = -\delta F_V / \delta u_{ij}$ satisfies the mechanical equilibrium equation, $\partial \sigma_{ij} / \partial x_j = 0$. The most evident consequence of the flexocoupling is the inhomogeneous terms in the boundary conditions (5).

Note that the application of the LGD-type continuum theory for the description of acoustic phonon dispersion for enough long waves with wave vectors $k < 1\,\text{nm}^{-1}$ does not require any special justifications as it is widely used in the literature (see e.g., Refs.[12 – 17, 19, 31-35, 47-48] and paragraph 3.2 in Ref.[49]) and well the results obtained from LGD theory agree with experimentally measured phonon spectra [31-35, 48]. For shorter waves with $k > 1\,\text{nm}^{-1}$ the results presented below

have only qualitative significance, but we hope that semi-quantitative description of the SAWs can be sufficient to stimulate the search of their experimental verification.

III. ANALYTICAL SOLUTION FOR A LOST SURFACE WAVE

A. Explicit form of the Euler-Lagrange boundary problem for transverse surface waves

Let us consider the transverse wave of electric polarization $P_2(x_1,x_3,t)$ and elastic displacement $U_2(x_1,x_3,t)$ propagating along direction x_1 near the surface $x_3=0$ of a semi-infinite non-piezoelectric solid [see **Fig. 1**]. The wave is not damped by the depolarizing effects influence because $div\vec{P}(x_1,x_3,t)=0$.

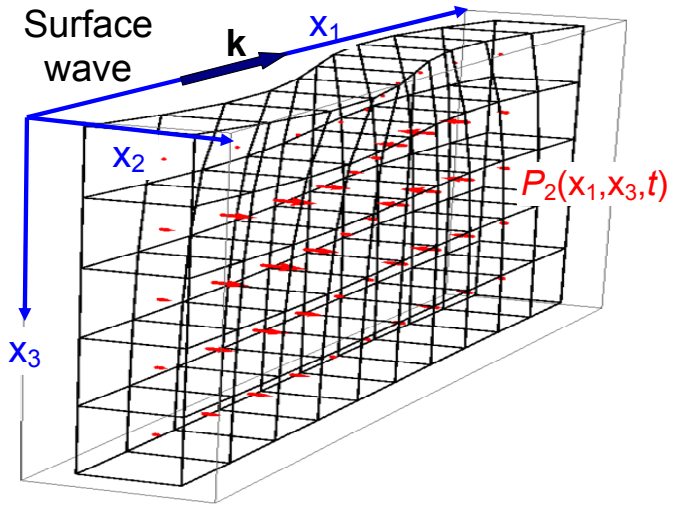

FIG. 1. Geometry of the surface wave propagating in a semi-infinite non-piezoelectric (dielectric or paraelectric) material. Red arrows are the elementary dipoles, which are zero at the surface in the particular case $\alpha_{S0}=\infty$ (because $P_2(x_1,0,t)=0$ at $\alpha_{S0}=\infty$). Black grid illustrates the deformation of the unit cells caused by the displacement $U_2(x_1,x_3,t)$ (the scale is distorted).

Explicit form of the E-L equations (4) for the purely transverse surface waves with the boundary conditions at the surface $x_3=0$ are derived in **Appendix A** of the **Suppl. Mat** [53]**.** These equations can be linearized in dielectrics and paraelectrics (i.e., at $\alpha>0$). For considered geometry the linearized E-L equations along with the boundary conditions (5) acquire relatively simple form (compare with the equations in paragraph 3.2 in Ref.[49]):

$$\rho\frac{\partial^2 U_2}{\partial t^2}+M\frac{\partial^2 P_2}{\partial t^2}-\Delta\left(c_{44}U_2+f_{44}P_2\right)=0 \qquad (6a)$$

$$\mu\frac{\partial^2 P_2}{\partial t^2}+M\frac{\partial^2 U_2}{\partial t^2}+\alpha P_2-\Delta\left(g_{44}P_2+f_{44}U_2\right)=0 \qquad (6b)$$

Symbol Δ stands for Laplace operator. Boundary conditions (5) acquire the form

$$\left(c_{44}\frac{\partial U_2}{\partial x_3} + f_{44}\frac{\partial P_2}{\partial x_3} \right)\Bigg|_{x_3=0} = 0, \qquad \left(\alpha_{S0}P_2 - g_{44}\frac{\partial P_2}{\partial x_3} - f_{44}\frac{\partial U_2}{\partial x_3} \right)\Bigg|_{x_3=0} = 0. \tag{6c}$$

Hereinafter the inequality $f_{44}^2 < c_{44}g_{44}$ is regarded valid for the system stability.

B. General expressions relating the amplitudes, frequency dispersion and penetration depth of the travelling surface waves

Let us look for the solution of the linearized boundary problem (6) in the form of a travelling surface wave:

$$P_2(x_1, x_3, t) = \exp(i(kx_1 - \omega t) - \xi x_3)\tilde{p}(k), \quad U_2(x_1, x_3, t) = \exp(i(kx_1 - \omega t) - \xi x_3)\tilde{u}(k). \tag{7}$$

Here k is the wave vector in the direction of the wave propagation, ω is its frequency, ξ is inverse penetration depth of the wave. Since the solid occupies the semi-space $x_3 \geq 0$, only the exponents either vanishing or not increasing at $x_3 \to \infty$ are present, so that the inequality $\mathrm{Re}(\xi) \geq 0$ should be valid.

The substitution of expressions (7) in Eqs.(6) leads to the system of linear algebraic equations for the amplitudes $\tilde{p}$ and $\tilde{u}$

$$\begin{cases} \left(\rho\omega^2 + c_{44}\left(\xi^2 - k^2\right)\right)\tilde{u} + M\omega^2\tilde{p} + f_{44}\left(\xi^2 - k^2\right)\tilde{p} = 0, \\ \left(\mu\omega^2 - \alpha + g_{44}\left(\xi^2 - k^2\right)\right)\tilde{p} + M\omega^2\tilde{u} + f_{44}\left(\xi^2 - k^2\right)\tilde{u} = 0. \end{cases} \tag{8}$$

The condition of the system (8) zero determinant gives the condition of the SAW existence

$$\left(\rho\omega^2 + c_{44}\left(\xi^2 - k^2\right)\right)\left(\mu\omega^2 - \alpha + g_{44}\left(\xi^2 - k^2\right)\right) = \left(M\omega^2 + f_{44}\left(\xi^2 - k^2\right)\right)^2. \tag{9}$$

The solution of Eq.(9) for the penetration depth of the wave is

$$\xi_{1,2}^2 = k^2 + \frac{-B(\omega) \pm \sqrt{B^2(\omega) - 4\left(c_{44}g_{44} - (f_{44})^2\right)C(\omega)}}{2\left(c_{44}g_{44} - (f_{44})^2\right)}, \tag{10a}$$

wherein the functions $B(\omega)$ and $C(\omega)$ are given by expressions

$$B(\omega) = \left(\mu\omega^2 - \alpha\right)c_{44} + \rho\omega^2 g_{44} - 2M\omega^2 f_{44}, \tag{10b}$$

$$C(\omega) = \rho\omega^2\left(\mu\omega^2 - \alpha\right) - \left(M\omega^2\right)^2. \tag{10c}$$

The conditions $c_{44}^2 R^2(k) \geq 4\left(\rho\omega^2 - c_{44}k^2\right)^2$ and $\dfrac{(c_{44}\mu + g_{44}\rho - 2M f_{44})\omega^2 - \alpha(T)c_{44}}{\left(c_{44}g_{44} - f_{44}^2\right)} - 2k^2 < 0$ are required for $\mathrm{Re}(\xi_i) \geq 0$.

Substitution of the solution (7) rewritten in the explicit form $Q_2 = [q_1\exp(-\xi_1 x_3) + q_2\exp(-\xi_2 x_3)]\exp[i(kx_1 - \omega t)]$ (where the symbol q=p for polarization P or q=u for the strain field U) to the Eqs.(8) and boundary conditions (6c) leads to the two independent equations for the penetration depths ξ_i:

$$\xi_1 = \xi_2, \tag{11a}$$

$$\alpha_{S0}\left(\rho\omega^2 - c_{44}k^2 - c_{44}\xi_1\xi_2\right) = (\xi_1 + \xi_2)\xi_1\xi_2\left(c_{44}g_{44} - (f_{44})^2\right). \tag{11b}$$

Along with Eqs.(11) the following relation between the amplitudes *p* and *u* should be valid,

$$u_i = -\left(\frac{M\,\omega^2 + f_{44}\left(\xi_i^2 - k^2\right)}{\rho\omega^2 + c_{44}\left(\xi_i^2 - k^2\right)}\right)p_i. \tag{12}$$

If the shear strain wave is excited by polarization, its resonant enhancement at definite frequency ω is possible under the condition $\rho\omega^2(k) + c_{44}\left(\xi_i^2[k,\omega(k)] - k^2\right) = 0$. The dispersion law $\omega(k)$ will be derived and analyzed below.

The evident form of Eq.(11a) is equivalent to the condition of zero determinant in Eq.(10a), namely

$$B^2(\omega) - 4C(\omega)\left[c_{44}g_{44} - (f_{44})^2\right] = 0. \tag{13}$$

Note, that the solution of Eq.(13) with respect to frequency is independent on the wave vector. Solution with a similar property was found by Romeo et al [17], who noted that for the case the "frequency dispersion" is limited to the discrete set of frequency values $\omega_n(k_n)$, which unlikely has chances to be observed.

Really in the secular case $\xi_1 = \xi_2 = \xi$ (Eq.(11a)) the expressions (7) for the solution should be modified as $P_2 = (p_1 - p_2\xi x_3)\exp(i(kx_1 - \omega t) - \xi x_3)$ and $U_2 = (u_1 - u_2\xi x_3)\exp(i(kx_1 - \omega t) - \xi x_3)$. A detailed consideration of the secular case, presented in the part D of **Suppl. Mat.** [53]**,** leads to the conclusion that the surface wave can exist under the validity of a very specific boundary condition, $\alpha_{S0} = 0$. Since it exists for a definite frequency, the solution (11a) is the "isolated" point that unlikely has chances to be observed experimentally.

C. Impact of the boundary conditions for polarization on the surface waves existence

In contrast to the pessimistic scenario of the experimental verification of the secular case (11a), the solution of Eq.(11b) has sense at all values of α_{S0} and can be simplified for two limiting cases, $\alpha_{S0} = 0$ and $\alpha_{S0} = \infty$, considered below.

(a) "Bulk-like" case I corresponds to the natural boundary conditions for polarization at the surface, which are zero normal derivative, $\partial P_2/\partial x_3\big|_{x_3=0} = 0$, since $\alpha_{S0} = 0$. Mathematically the case I is equivalent to the condition $\xi_1\xi_2 = 0$, because $\xi_1 + \xi_2 \neq 0$. Setting $\xi = 0$ in Eq.(9) we immediately obtain the dispersion relation

$$\left(\rho\omega^2 - c_{44}k^2\right)\left(\mu\,\omega^2 - \alpha - g_{44}k^2\right) = \left(M\,\omega^2 - f_{44}k^2\right)^2. \tag{14}$$

In fact Eq. (14) represents the dispersion relation for a transverse phonon mode in the bulk, because its decay factor ξ given by Eqs.(10) is zero. As anticipated Eq.(14) coincides with Eq.(13b) from Ref.[47] in a paraelectric phase with $P_S = 0$ and $2\alpha \to \alpha$ (due to the absence of factor ½ in the free energy in Ref.[47]).

(b) SAW case II corresponds to zero polarization at the surface, $P_2(x_1,0,t) = 0$, since $\alpha_{S0} = \infty$ and thus $\rho\omega^2 - c_{44}k^2 - c_{44}\xi_1\xi_2 = 0$ from Eq.(11b). The latter condition jointly with the condition $p_1 = -p_2$ is sufficient to satisfy the boundary conditions (6c). The dispersion relation obtained from Eqs.(11b) and (10a) is

$$\frac{\left(\rho\omega^2 - c_{44}k^2\right)^2}{c_{44}^2} = \frac{\left(\rho\omega^2 - c_{44}k^2\right)\left(\mu\omega^2 - \alpha - g_{44}k^2\right) - \left(M\omega^2 - f_{44}k^2\right)^2}{c_{44}g_{44} - \left(f_{44}\right)^2}. \qquad (15)$$

The most important is that under the absence of static ($f_{44} = 0$) and dynamic ($M = 0$) flexocoupling the dispersion relation (15) reduces to the bulk dispersion law, $\rho\omega^2 = c_{44}k^2$, excluding the separate frequency point $\frac{\rho\omega^2}{c_{44}} = \frac{\mu\omega^2 - \alpha}{g_{44}}$. In the presence of flexoelectric coupling the explicit form of Eq.(15) is a biquadratic equation

$$A(k)\omega^4 - Q(k)\omega^2 + \frac{\alpha c_{44}k^2}{c_{44}g_{44} - f_{44}^2} = 0, \qquad (16a)$$

where the functions $Q(k) = \frac{\alpha\rho}{c_{44}g_{44} - f_{44}^2} + \left(\frac{g_{44}\rho + c_{44}\mu - 2M f_{44}}{c_{44}g_{44} - f_{44}^2} - 2\frac{\rho}{c_{44}}\right)k^2$ and $A(k) = \frac{\rho\mu - M^2}{c_{44}g_{44} - f_{44}^2} - \frac{\rho^2}{c_{44}^2}$ are introduced. Since $c_{44}g_{44} > f_{44}^2$ for the system stability, and $\alpha > 0$ for dielectrics and paraelectrics, the last term in Eq.(16a) are positive for the these materials. Since we regard that $\rho\mu > M^2$ for the Lagrangian (2) stability, the first term $A(k)$ can be of arbitrary sign, but inevitably becomes positive under the condition $f_{44}^2 \to c_{44}g_{44}$, i.e., when the flexoelectric coefficient increases towards the critical value. Under the condition $Q(k) > 0$ and relatively high f_{44}^2 Eq.(16a) has two roots, a transverse optic (**TO**) and acoustic (**TA**) mode. At $Q(k) < 0$ and $A(k) < 0$ it contains only one TA mode. Corresponding equation for the decay factors can be derived from Eqs.(9)-(10), namely,

$$\xi^4 + R(k)\xi^2 + \frac{\left(\rho\omega^2 - c_{44}k^2\right)^2}{c_{44}^2} = 0, \qquad (16b)$$

where the function $R(k)=\dfrac{(c_{44}\mu+g_{44}\rho-2M f_{44})\omega^2-\alpha(T)c_{44}}{(c_{44}g_{44}-f_{44}^2)}-2k^2$ is introduced. Since the last term in Eq.(16b) is positive because of $c_{44}g_{44}>f_{44}^2$, the conditions for which both decay factors ξ_i become real are $R(k)<0$ and $c_{44}^2R^2(k)\geq 4\left(\rho\omega^2-c_{44}k^2\right)^2$. Both ξ_i are complex in the case $c_{44}^2R^2(k)<4\left(\rho\omega^2-c_{44}k^2\right)^2$, and purely imaginary under the conditions $c_{44}^2R^2(k)\geq 4\left(\rho\omega^2-c_{44}k^2\right)^2$ and $R(k)>0$.

Expressions (13)-(16) are the formal analytical solution of the considered problem, but only Eqs.(16) (being the explicit form of Eq.(15)) contain the "lost" transverse surface wave induced by the flexoelectric coupling, which we abbreviated as **Flexo-SAWs** below. The existence of Flexo-SAWs is not limited to a particular material, but for the sake of concreteness, we have chosen a well-studied quantum paraelectric $SrTiO_3$ (**STO**) for which the majority of constants are known. Below we explore the wave dispersion in a transverse direction and its penetration under the STO surface.

IV. FLEXOCOUPLING IMPACT ON SURFACE WAVES PROPERTIES IN NON-PIEZOELECTRIC SOLIDS

A. Frequency dispersion, phase velocity and penetration depth of SAWs in $SrTiO_3$

Using Eqs.(16) we calculated the frequency dispersion $\omega(k)$ of the travelling wave vector for the case of paraelectric STO at temperatures (100 – 400) K. TA and TO modes penetrating in the bulk were calculated from Eq.(14). Most of STO material parameters are well-known. Numerical values of the unknown STO parameters have been extracted from the fitting [48] of phonon spectra obtained from the inelastic neutron scattering [21]. STO parameters are listed in **Table I.** Using the-parameters and the detectable limit of displacement fluctuation amplitude $U_2 \sim$ 1pm we obtained the value of polarization amplitude $P_2 \sim 0.05\,\mathrm{C/m^2}$ from Eq.(12).

Table I. Description, dimension and numerical values of parameters in Eqs.(16) collected from Refs. [54, 55, 56, 57]

Description of the physical parameter	**Symbol and dimension**	**Numerical value for $SrTiO_3$**	**Refs**
Coefficient at P^2	$\alpha(T)$ ($\times$C$^{-2}\cdot$m J)	$\alpha_T\left(T_q\coth\left(T_q/T\right)-T_C\right)$	50
Inverse Curie-Weiss constant	α_T ($\times10^5$C$^{-2}\cdot$m J/K)	15	54 - 57
Curie temperature	T_C (K)	30	54 - 57
Characteristic temperature	T_q (K)	54	54 - 57
Surface energy coefficient	α_{S0} ($\times$C$^{-2}\cdot$J)	∞	N/A
LGD-coefficient at P^4	β ($\times10^8$ JC$^{-4}\cdot$m^5)	81	54 - 57
LGD-coefficient at P^6	γ ($\times10^9$JC$^{-6}\cdot$m^9)	0	54 - 57

Electrostriction coefficient	q_{44} ($\times 10^9$ J m/C^2)	2.4	54, 57
Elastic stiffness coefficient	c_{44} ($\times 10^{10}$ Pa)	11	54 - 57
Gradient coefficient at $(\nabla P)^2$	g_{44} ($\times 10^{-10}$C^{-2}m^3 J)	0.5 (fitting parameter)	48,
Elastic strain gradient $(\nabla u)^2$	v ($\times 10^{-9}$V s^2/m^2)	0 (fitting parameter)	this work
Static flexoelectric coefficient	f_{44} (V)	+2.1 (exp. value)	48
Dynamic flexoelectric coefficient	M ($\times 10^{-8}$Vs^2/m^2)	–1 (fitting parameter)	48
Kinetic coefficient	μ ($\times 10^{-18}$s^{2}m J)	1.45 (fitting parameter)	48
Material density at norm. cond.	ρ ($\times 10^3$ kg/m^3)	4.930 at 120 K	handbook
Lattice constant	a (nm)	a_x=a_y=a_z=0.395 at 120 K	handbook

The dispersion curves of the lowest transverse acoustic (TA) and transverse optic (TO) surface phonon modes are shown by solid curves in **Fig. 2(a)**. The frequency of TO mode is rather high, and the minimal distance between the TO and TA modes is about 5 THz at $k \approx 1.2\,\mathrm{nm}^{-1}$. The modes interaction is very weak in STO that is typical for paraelectrics. For the sake of comparison the dispersion corresponding to the bulk TA and TO phonon modes are presented by dashed curves in **Fig. 2(a)**. The difference between the dispersion curves for the bulk and surface TO modes is the most pronounced (~ (2 – 5)THz) for small wave vectors $k < 0.5\,\mathrm{nm}^{-1}$ but remains essential for all considered values $0 \le k \le 5\,\mathrm{nm}^{-1}$. The difference between the frequency dispersion of the bulk and surface TA modes becomes noticeable only for the wave vector values $k > 2$ nm^{-1}. Thus the differences between the bulk and surface TO modes decreases, while the differences between the bulk and surface TA modes increases with the temperature increase [compare solid and dashed curves of different colors in **Fig. 2(a)**].

Despite the difference between the frequency dispersion of the surface and bulk TA modes are essentially smaller than between ~~the~~ corresponding TO modes, further we limit our consideration by surface TA modes properties, primary because their penetration depth is real [**Fig. 2(c)**] and the acoustic frequency is much lower that the optical one [**Fig. 2(a)**]. These properties of surface TA modes open the interesting possibilities for their excitation and experimental observation. In contrast, it appeared that TO modes penetration depth is purely imaginary for STO ($\xi = iq_z$) and so they are not localized near the surface. In particular the TO mode calculated from Eqs.(16) is a standing waves reflected from the surface $x_3 = 0$, and it disappears with the flexocoefficient f_{44} decrease below 1.5 V. As a matter of fact the impact of the flexocoupling on the standing TO waves requires a separate study, because their amplitude can be noticeable in thin films [see the next section].

The dependences of the surface TA wave penetration depths $1/\xi_1$ and $1/\xi_2$ on the wavelength λ are shown in **Fig. 2(b)** for several temperatures (100 – 400) K. Because the penetration depth $1/\xi_1$ rapidly increases with the wavelength increase [see solid curves in **Fig. 2(b)**], the surface wave properties gradually tend to the ones of bulk wave in the limit $\lambda \to \infty$. The depth $1/\xi_2$ firstly increases, then reaches a very smooth maximum (or a plateau) and then saturates with the

temperature decrease. Both penetration depths $1/\xi_1$ and $1/\xi_2$ almost coincide at small $\lambda < 1$ nm [compare dashed and solid curves in **Fig. 2(b)**]. Note that the depth $1/\xi_1$ monotonically increases with the temperature increase; and the depth $1/\xi_2$ decreases with the temperature decrease [compare black, red, purple and blue dashed curves in **Fig. 2(b)**]. Since the depths determine the localization of the surface wave, only the highest value $1/\xi = \max[1/\xi_1, 1/\xi_2]$ matters.

Dispersion law for Rayleigh, Bleustein and Gulyaev waves are similar to the bulk elastic (infrasound, acoustic or ultrasound) waves. Their frequency ω is proportional to the wave number, k, namely $\omega = v_P k$, where v_P is the wave velocity. The dependence of the surface TA wave phase velocity $v_P = \omega/k$ on its wavelength $\lambda = 2\pi/k$ is shown in **Fig. 2(c)** for several temperatures from the range (100 – 400) K. Firstly the phase velocity increases enough sharply and monotonically with the wavelength increase from 0.1nm to 10 nm, and then it saturates and tends to the phase velocity of the shear wave in the bulk of material. Smaller v_P values correspond to the lower temperatures [compare black, red, purple and blue curves in **Fig. 2(c)**]. The saturation starts at λ values about 5 nm for T = 400 K, and about 30 nm for T = 100 K.

The frequency spectrum of the phase velocity is shown in **Fig. 2(d)** for several temperatures (100 – 400) K. The velocity monotonically decreases with the frequency increase at frequencies less than the critical value ω_{cr}, at that $\omega_{cr} \approx 3.7$ THz at 100 K and $\omega_{cr} \approx 8.75$ THz at 400 K (compare black, red, purple and blue curves in **Fig. 2(d)**). At frequencies $\omega > \omega_{cr}$ the velocity is zero; hence the second-order phase transition occurs at $\omega = \omega_{cr}$. Numerical values of the phase velocity ~(1 – 4)km/s are in the same interval than the SAW velocity (3472.5 ± 1.5) m/sec measured by Soffer et al [28] at the nonpolar Y-cut of piezoelectric $LiNbO_3$. Soffer waves are typical manifestation of Bleustein and Gulyaev SAWs. However considered SAWs have the eigen frequencies $\omega(k) \sim 5$ THz at the wave vectors $k = (1 – 100)$ nm^{-1}, while the SAWs in $LiNbO_3$ were excited at resonant frequency about 40 MHz at $k = 0.1$mm^{-1}. The several orders of magnitude difference calls into question the opportunity to observe and study Flexo-SAWs in paraelectrics using the optical spatial filtering technique [28].

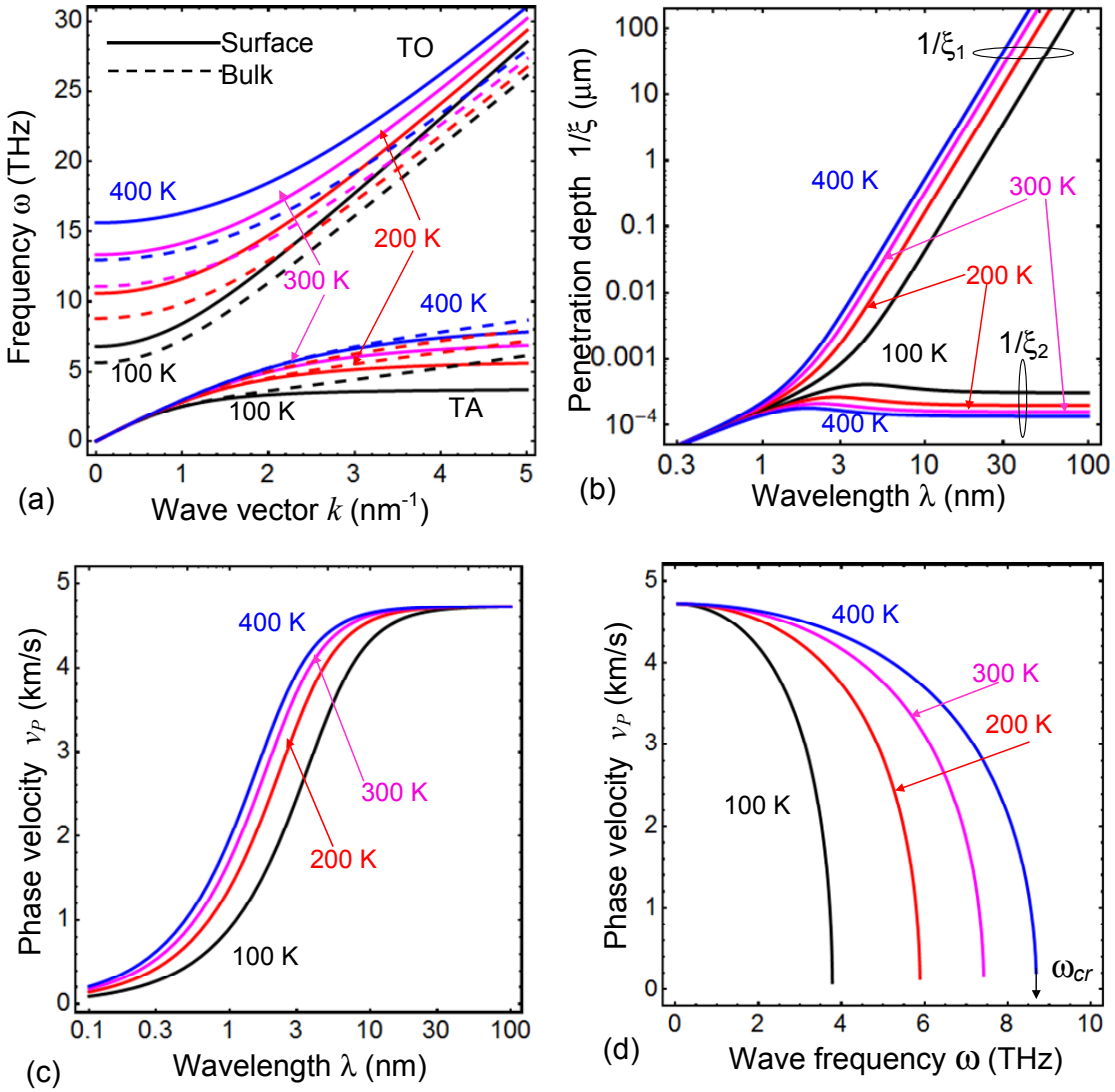

FIG. 2. (a) Frequency dispersion of the bulk (dashed curves) and surface (solid curves) phonon modes calculated for STO parameters. Transverse optic ("TO") and acoustic ("TA") modes are shown. **(b)** Dependence of penetration depth of the surface TA wave on its wavelength. **(c)** Phase velocity of the surface TA wave in dependence on the wavelength. **(d)** Phase velocity dependence on the surface wave frequency. Different curves in parts **(a)-(d)** correspond to the temperatures T=100, 200, 300 and 400 K, which values are specified near the curves. Static flexoelectric coefficient f_{44}=2.1 V, dynamic flexocoupling constant $M = -1\times10^{-8}\mathrm{Vs}^2/\mathrm{m}^2$, surface energy parameter $\alpha_{S0} = \infty$. Other material parameters of STO are listed in **Table I.**

B. Impact of the flexocoupling on the SAW frequency dispersion and penetration depth

Note that **Fig. 2** is calculated for the static flexoelectric coefficient f_{44}=2.1 V and dynamic flexocoupling constant $M = -1\times10^{-8}\mathrm{Vs}^2/\mathrm{m}^2$ extracted from the soft phonon spectra measured by inelastic neutron scattering [see Fig.2 in Ref. [21]]. Note that the extracted value f_{44}=2.1 V is in a surprising agreement with the value f_{44}=(2.18±0.05) V determined from the bending of STO crystal

by Zubko et al [58], but earlier they measured that f_{44}=1.3 V [59]. The dynamic flexocoupling constant absolute value 1×10^{-8}Vs^2/m^2 is within the range $(0 - 20)\times10^{-8}$Vs^2/m^2 that's physical reasonability was estimated in Refs. [47, 48]. Since exact values of f_{ij} and M are still under debate for most of ferroics including ferroelectrics and quantum paraelectrics [60, 61, 62], it seems reasonable to explore the properties of the revealed surface TA wave on the value of f_{ij} varying in the actual range (0 – 3)V. Hereinafter we consider $M < 0$ for STO, because the inequality $Mf_{44} < 0$ is in a much better agreement with the phonon spectra [21, 22, 23] and bending measurements [58] than the case $M f_{44} > 0$. Results are presented in **Figs 3** and **4**. The case M=0 is shown in the figures for comparison.

Figure 3(a) shows the dependences of the SAW penetration depth $1/\xi$ on the static flexocoelectric efficient f_{44} calculated for several wave vectors k_n, zero ($M = 0$) and negative ($M < 0$) dynamic flexoconstants, respectively. Under the condition $M = 0$ the penetration depth $1/\xi$ sharply increases (up to cm) with the flexoelectric coefficient f_{44} decrease below 0.5 V and diverges when its value tends to zero [see dashed curves in **Fig. 3(a)**]. When the penetration depth $1/\xi$ diverges, the surface wave properties coincide with the ones of a bulk wave. For wave vectors $k > 1$ nm^{-1} and $1\text{V} < f_{44} < f_{44}^{cr}$ the TA wave penetration depth $1/\xi$ becomes less than 100 nm, so it is indeed becomes a SAW. The depth $1/\xi$ very sharply increases (up to the infinity) in the immediate vicinity of $f_{44} \to f_{44}^{cr}$, and becomes imaginary at $f_{44} > f_{44}^{cr}$ indicating the onset of the spatially modulated phase. The critical value of the spatially modulated phase appearance is $f_{44}^{cr} = \sqrt{g_{44}c_{44}} \approx 2.45$ V, and it is independent on the dynamic flexocoupling value as anticipated [48]. The divergence of $1/\xi$ at $f_{44} = 0$ disappears for negative M and positive f_{44}. Corresponding curves have a sharp maximum only at f_{44}^{cr} [see solid curves in **Fig. 3(a)**]. Actually we established that the divergence $1/\xi$ can originate from the last term $\left(M\omega^2 - f_{44}k^2\right)^2$ in Eq.(15) for the TA mode frequency ω. Since the term is positive for the case $f_{44}M < 0$, corresponding penetration depths given by Eqs.(10) are finite. Negative sign of f_{44} induces the additional divergence of $1/\xi$ at negative M values. At the same time the inequality $M f_{44} > 0$ seem in a contradiction with the values extracted from the neutron scattering [22, 23] and bending [58] experiments in STO. However the condition $M f_{44} \geq 0$ and is far not excluded for other materials.

Figure 3(b) shows the dependence of the TA mode frequency ω on the static flexoelectric coefficient f_{44}, calculated for the cases $M = 0$ and $M < 0$, respectively. The difference between these two cases is relatively small [compare solid and dashed curves in **Fig. 3(b)**], leading to the conclusion that the impact of dynamic flexoconstant value on the frequency ω of surface TA mode is

relatively small (at least in comparison with its influence on the penetration depth). For both cases M=0 and M<0 the frequency ω becomes higher than 2.5 THz for small wave vectors $k \geq 0.5$ nm^{-1} and flexocoefficients f_{44} lying in the range (0 – 3) V. The frequency values are relatively high (>4 THz) and almost independent on the flexoelectric coefficient f_{44} for wave vectors $k < 1$ nm^{-1}, it starts to decrease slowly with f_{44} increasing for $k > 1$ nm^{-1}. Note that THz values are typical for the soft phonons frequencies in proper and incipient ferroelectrics.

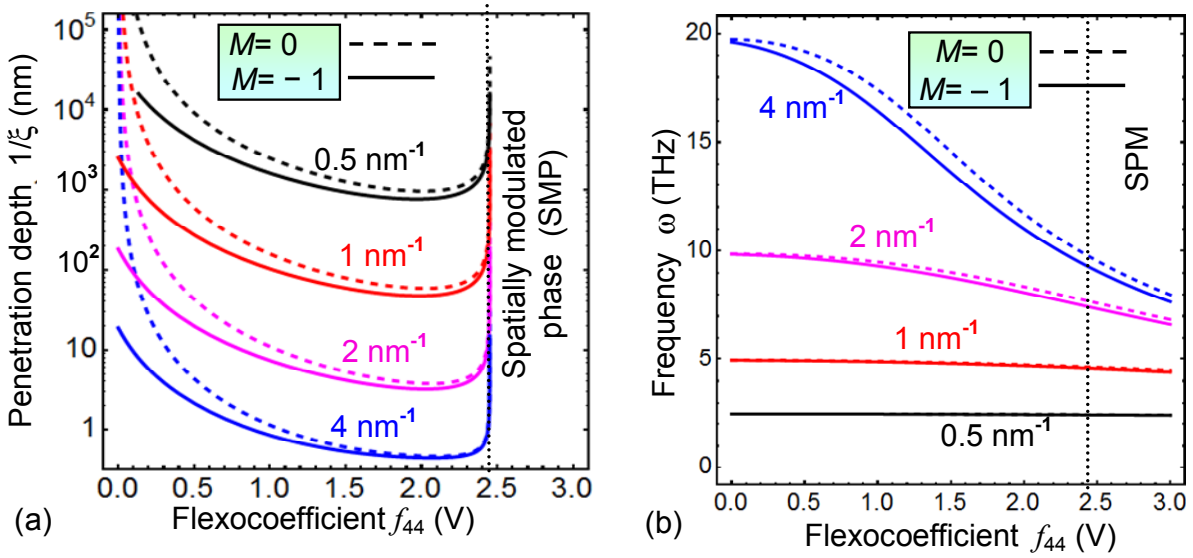

FIG. 3. Dependence of the TA wave penetration depth $1/\xi$ **(a)** and frequency ω **(b)** on flexocoefficient f_{44} calculated at 300 K for $M = 0$ (dashed curves) and $M = -1\times10^{-8}$Vs^2/m^2 (solid curves). Different curves correspond to the wave vectors $k = (0.5, 1, 2, 4)$ nm^{-1} specified near the curves. STO parameters are listed in **Table I.**

Figures 4(a) and **4(b)** demonstrate the dependences of the SAW penetration depth $1/\xi$ on the flexoelectric coefficient f_{44} and wave vector k calculated for the cases $M = 0$ and $M < 0$, respectively. Under the condition $M = 0$ the penetration depth $1/\xi$ sharply increases (up to cm) with the flexoelectric coefficient f_{44} decrease below 0.5 V and diverges when its value tends to zero [see different contour lines in **Fig. 4(a)**]. The divergence of $1/\xi$ at $f_{44} = 0$ disappears for negative M and positive f_{44}. Corresponding curves have a sharp maximum at f_{44}^{cr} only [see different contour lines in **Fig. 4(b)**].

Figures 4(c) and **4(d)** show the dependence of the surface TA mode frequency ω on the flexoelectric coefficient f_{44} and wave vector k calculated for the cases $M = 0$ and $M < 0$, respectively. The difference between these cases is relatively small. For both M=0 and M<0 the frequency ω becomes higher than 1 THz for small wave vectors $k \geq 0.2$ nm^{-1} and flexocoefficient 0<f_{44}<3 V. The

frequency ω is almost independent on f_{44} for wave vectors $k < 1$ nm^{-1} [see almost vertical contour lines of constant ω in **Figs.4(c)** and **4(d)**]. Under the condition $k > 1$ nm^{-1} the frequency relatively slowly and monotonically decreases with f_{44} increase [**Figs. 4(c)** and **4(d)**].

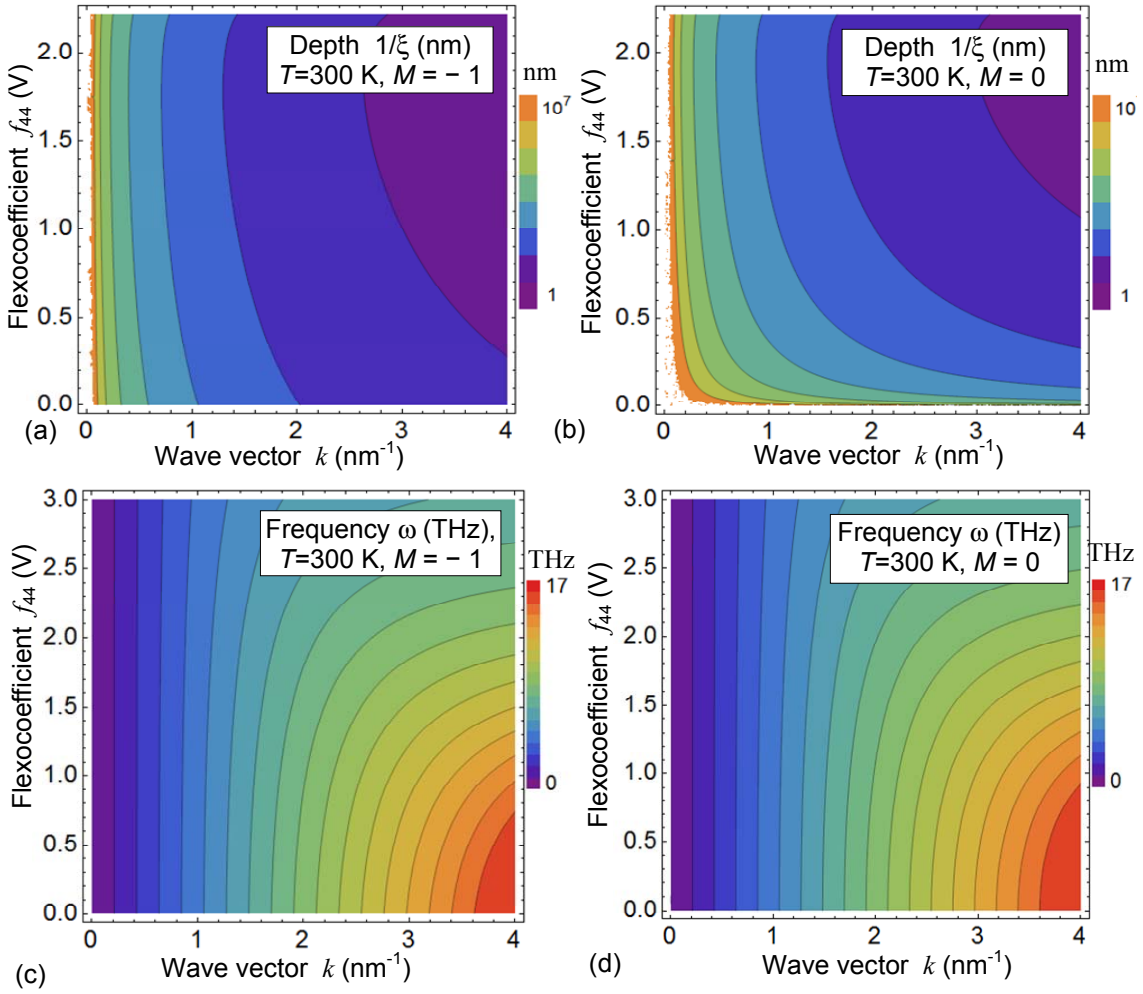

FIG. 4. Contour maps of the TA mode penetration depth $1/\xi$ **(a, b)** and frequency ω **(c,d)** in coordinates "wave vector k – flexoelectric coefficient f_{44}" calculated for $T = 300$ K $M = -1\times10^{-8}$Vs^2/m^2 **(a, c)** and M=0 **(b, d)**. Parameters corresponding to STO are listed in **Table I.**

To resume the analyses of the graphical results presented in section IV we can state that the existence and penetration depth of the revealed surface TA phonon mode is ruled by the static and dynamic flexocouplings. In particular the mode transforms to the bulk wave in the absence of the couplings. So the flexoelectricity indeed generates previously unexplored type of acoustic waves, further abbreviated as **Flexo-SAWs**, which can travel near the flat surface of any solid. Next we can speculate whether these surface waves be excited and detected separately from the classical bulk phonon modes.

VI. POSSIBILITIES OF FLEXO-SAWS EXCITATION AND EXPERIMENTAL OBSERVATION

Since the calculated frequency dispersion $\omega(k)$ of the Flexo-SAW is within THz region for the wave vectors in the range k=(0.05 – 5)nm^{-1} in non-piezoelectric paraelectrics with relatively small coefficient $\alpha \cong 1/\varepsilon_0\varepsilon$ (corresponding to the high relative dielectric permittivity $\varepsilon \geq 100$), the waves can be excited similarly to the bulk acoustic phonons, and the dispersion $\omega(k)$ can be determined from inelastic neutron scattering [21, 22]. For instance the dispersion curves of the bulk and surface TO and TA modes in STO are shown in **Fig. 5(a)** for the actual range of neutron energies ($5\text{meV} \leq 2\pi\hbar^2k^2/m_n \leq 50\text{meV}$) and different temperatures ($100 \leq T \leq 400$ K).

We expect that the peaks of inelastic neutron scattering intensity corresponding to the surface and bulk phonon modes can be separated in thin non-piezoelectric paraelectric layers, where the phonon spectra near the surface becomes more and more important with the thickness decrease, and corresponding peak either splits, or shifts. This is possible because the difference between the energy of the surface and bulk phonons is $\Delta E_{TO}(k) = (1 - 3)$ meV for TO modes at k =(0.1 – 5)nm^{-1}, and $\Delta E_{TA}(k) = -(0.5 - 3)$ meV for TA modes at k>2nm^{-1} at temperatures (100 – 300) K [see **Fig. 5(c)**]. Corresponding penetration depth of TA mode $\xi^{-1}(k)$ is about or less than 10 nm at k>1 nm^{-1} and T=100 K, and at k>2 nm^{-1} and T=300 K [see **Fig. 5(b)**]. So that we expect that the surface and bulk phonon modes can be separated in thin non-piezoelectric layers with thickness of about several penetration depths, which is about or less than 50 nm for STO. In thin layers both surfaces contribute into the response. For a macroscopic sample each peak position corresponds to the response of each bulk acoustic or optic mode, which positions are well-known for many ferroics and typically tabulated (e.g. for STO).

TO modes, which "penetration depth" appeared purely imaginary for STO parameters [see **Fig. 5(d)**], can be imagined as standing TO waves reflected from the surface $x_3 = 0$. As it was mentioned, TO mode disappears with the flexocoefficient f_{44} decrease below 1.5 V. The standing TO waves are expected to be noticeable in thin films, which thickness is an integral multiple of their period $2\pi/q_z(k)$.

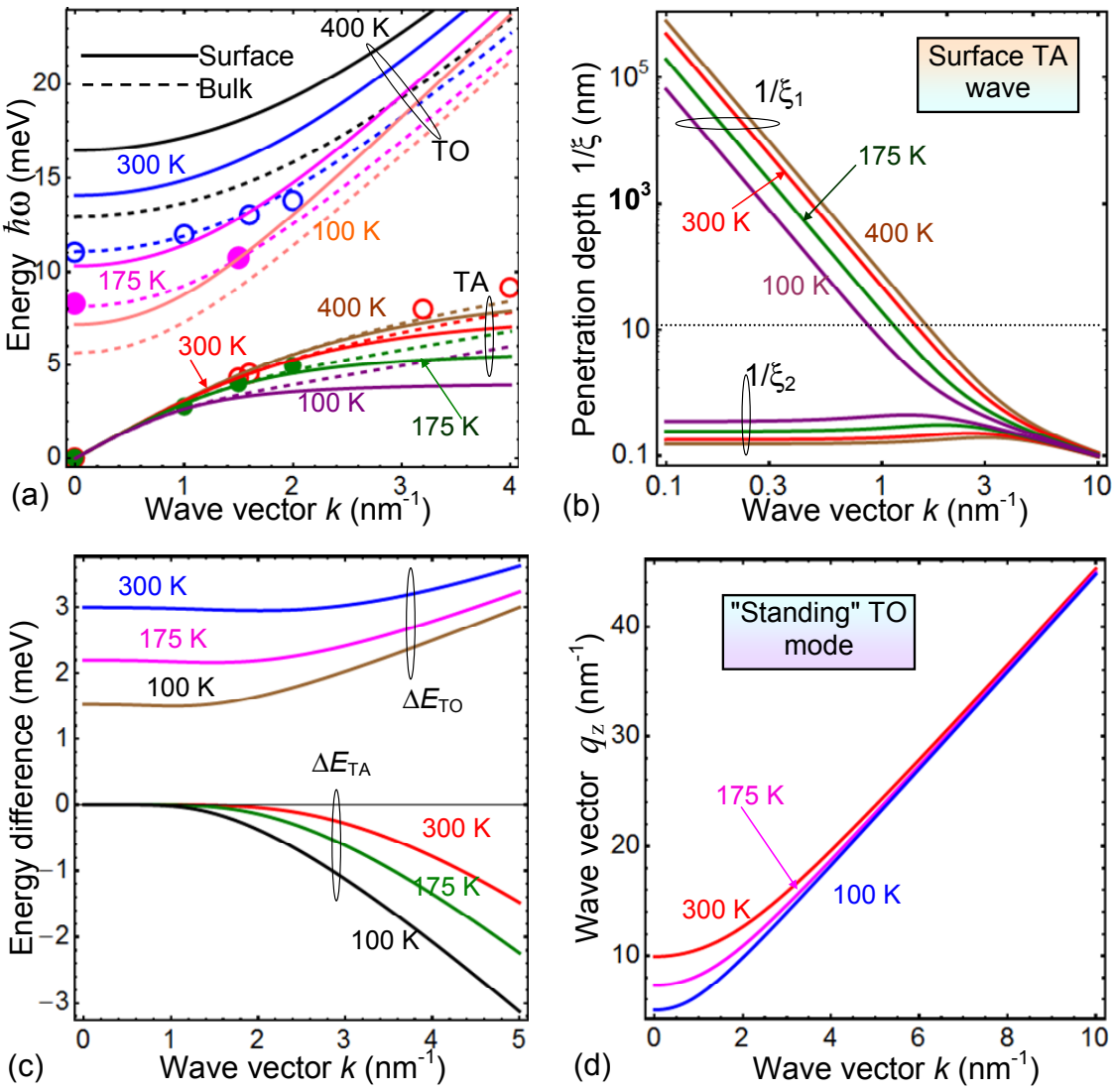

FIG. 5. (a) Energy dispersion $\hbar\omega(k)$ of the bulk (dashed curves) and surface (solid curves) phonon modes calculated in STO. Transverse optic ("TO") and acoustic ("TA") modes are shown. Symbols are initial experimental data from figure 2 in Ref. [21]. **(b)** Dispersion of the surface TA mode penetration depth $\xi^{-1}(k)$. Different curves in **(a)-(b)** correspond to the temperatures T=100, 175, 300 and 400 K, which values are specified near the curves. **(c)** Energy difference $\Delta E(k)$ of the surface and bulk TO modes (top curves with label ΔE_{TO}) and TA modes (bottom curves with label ΔE_{TA}). **(d)** Dispersion of the TO modes wave vector $q_z(k)$ in the direction x_3, normal to the surface. Corresponding localization depth is purely imaginary, $\xi = iq_z$. Different curves in parts **(c)-(d)** correspond to the temperatures T=100, 175 and 300 K, which values are specified near the curves. STO parameters obtained from the fitting of experimental data [21] are listed in **Table I.**

The dispersion of the TA shear strain wave amplitudes $u_i(k)$ calculated from Eq.(12) are shown in **Fig.6(a)**. The amplitude is normalized on the polarization amplitudes p_i regarded proportional to the applied electric field $\mathbf{E}_0$, $p_i \sim \chi_{ij} E_j^0$. Contour maps of amplitudes of polarization $P_2(x_1, x_3, t)$ and displacement $U_2(x_1, x_3, t)$ components in TA wave are shown in **Figs.6(b)** and **6(c)**, respectively. The maps were calculated from Eq.(7) for fixed frequency $\omega(k)$, time $t = 2\pi/\omega(k)$ and wave vector $k = 1$ nm^{-1}. As one can see from **Figs.6(b)** the polarization wave is zero at the surface $x_3 = 0$ for the case $\alpha_{S0} = \infty$, because $p_1 = -p_2$. The wave amplitude has a maximum at depth $x_3 \approx 2$ nm and becomes negligibly small at $x_3 > 15$ nm. Displacement is maximal at $x_3 = 0$ and exponentially vanishes at $x_3 > 5$ nm. So that the neutron scattering in thin STO films of thickness less than (20 – 50)nm should give us the information about the surface TA phonons coupled with flexoelectricity.

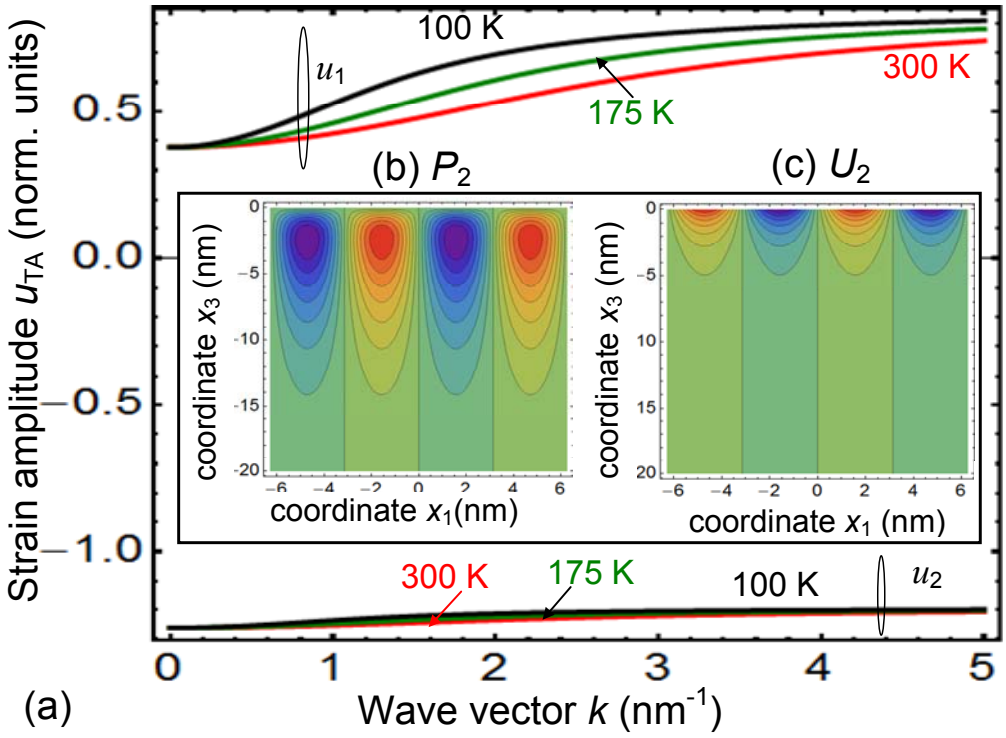

FIG. 6. (a) The dispersion of the normalized TA wave strain amplitudes $u_i[\omega(k), k]$ calculated in STO at temperatures 100, 175 and 300 K, which values ate shown near the curves. The amplitude is normalized on the polarization amplitudes p_i. Insets: contour maps of the TA wave amplitudes $P_2(x_1, x_3, t)$ **(b)** and $U_2(x_1, x_3, t)$ **(c)** calculated from Eq.(7) for fixed wave vector $k = 1$ nm^{-1} and time $t = 2\pi/\omega(k)$. STO parameters are listed in **Table I.**

To resume the section, the possibilities of the Flexo-SAWs observation by inelastic neutron scattering is much more favorable in thin layers (< 50 nm) of paraelectrics and incipient ferroelectric with dielectric permittivity $\varepsilon>>100$ (i.e. in STO or KTO at low temperatures) in comparison with linear low-k dielectrics with $\varepsilon\leq 10$. Also we hope that some of the predicted properties of Flexo-SAWs can be verified and explored using optical imaging, infrared spectroscopy, Raman and Brillouin scattering and Surface Enhanced Raman scattering based on the incomplete internal reflection. Also lattice dynamics calculations (complementary to LGD approach) can be in order, but unfortunately they are beyond our possibilities.

VII. CONCLUSION

The existence of the shear SAWs was regarded impossible in non-piezoelectrics with flat homogeneous surface without taking into account the flexoelectric coupling. We predict that shear transverse SAWs can propagate in all crystalline dielectrics with the flexoelectric coupling, and named them Flexo-SAWs. In particular, we predict that the Flexo-SAWs should have rather unusual dispersion properties, which main features are following:

1. The existence and penetration depth of the Fleo-SAW is ruled by the static and dynamic flexoelectric couplings. In particular, the penetration depth of acoustic mode is relatively small (several nm) for moderate and high values of the flexocoupling strength and diverges in the absence of the flexoelectric coupling, and in the latter case these waves become indistinguishable from the bulk waves.
2. With decreasing the wave vector k the wave velocity along the surface approaches the speed of bulk shear waves, while the penetration depth tends to infinity.
3. For wavelengths about micrometer order and less the phase velocity of the surface wave decreases, and its penetration depth increases up to tens of microns.
4. The dispersion relation for Flexo-SAW depends strongly on the boundary conditions for the electric polarization at the surface of the material.

Since the SAW transforms to the bulk wave in the absence of the couplings, we conclude that the flexoelectricity indeed generates previously unexplored type of SAWs, Flexo-SAWs, which can travel near the flat surface of any solid. The Flexo-SAW has THz frequency in a paraelectric $SrTiO_3$, and its penetration depth varies from nanometers to hundred microns depending on the wave vector varying from 0.1 nm^{-1} to 10 nm^{-1}.

We expect that the peaks of inelastic neutron scattering intensity corresponding to the Flexo-SAW and bulk phonon modes can be separated in the paraelectric layers of thickness less than (20 – 50) nm, giving an independent opportunity to define the flexoelectric coefficients, which are poorly

measured by other methods. The absence of the experimental observations of Flexo-SAWs can be explained by a very small neutron scattering intensity in thin layers.

In contrast to acoustic modes, it appeared that the penetration depth of transverse optic modes is purely imaginary for the strontium titanate and so they are not localized near the surface. In fact the mode is a standing wave reflected from the surface, and it disappears with the flexoelectric coefficient decrease. The impact of the flexocoupling on the standing waves deserves a separate theoretical study, because their amplitude can be noticeable in thin paraelectric films.

Authors' contribution. E.A.E. and A.N.M. contributed equally to the research idea, problem statement and analytical calculations; E.A.E. prepared graphics and A.N.M. wrote the manuscript draft. M.D.G. worked densely on the results analyses and discussion. S.V.K. contributed very significantly to the research motivation, results analyses and discussion, manuscript text and structure improvement.

Acknowledgements. Authors are very grateful to the Referees of the paper for the valuable remarks and suggestions, as well as for invaluable help with literature analysis.

REFERENCES

1 Pierre-Gilles De Gennes, "Wetting: statics and dynamics." *Reviews of modern physics* 57, no. 3: 827 (1985).

2 Vitaliy A. Shchukin, and Dieter Bimberg. "Spontaneous ordering of nanostructures on crystal surfaces." *Reviews of Modern Physics* 71, no. 4 (1999): 1125.

3 Lord Rayleigh «On Waves Propagated along the Plane Surface of an Elastic Solid». Proc. London Math. Soc. s1-17 (1): 4–11. (1885).

4 Zuliang Yu, and Siegfried Boseck. "Scanning acoustic microscopy and its applications to material characterization." *Reviews of Modern Physics* 67, no. 4: 863 (1995).

5 Kerstin Länge, Bastian E. Rapp, and Michael Rapp. "Surface acoustic wave biosensors: a review." *Analytical and bioanalytical chemistry* 391, no. 5: 1509-1519 (2008).

6 Mauricio M. de Lima Jr, and Paulo V. Santos. "Modulation of photonic structures by surface acoustic waves." *Reports on progress in physics* 68, no. 7: 1639(2005).

7 A. N. Alexeyev, and D. V. Roshchupkin. "Diffraction of surface acoustic waves on the zigzag domain wall in a $Gd_2(MoO_4)_3$ crystal." *Applied physics letters* 68, no. 2: 159-160 (1996).

8 Jürgen Schiefele, Jorge Pedrós, Fernando Sols, Fernando Calle, and Francisco Guinea. "Coupling light into graphene plasmons through surface acoustic waves." *Physical review letters* 111, no. 23: 237405 (2013).

9 Tanaka, Yukihiro, and Shin-ichiro Tamura. "Surface acoustic waves in two-dimensional periodic elastic structures." Physical Review B 58, no. 12 (1998): 7958.

10 E. S. K. Young, A. V. Akimov, M. Henini, L. Eaves, and A. J. Kent. "Subterahertz acoustical pumping of electronic charge in a resonant tunneling device." *Physical review letters* 108, no. 22: 226601 (2012).

11 Jean-Charles Beugnot, Sylvie Lebrun, Gilles Pauliat, Hervé Maillotte, Vincent Laude, and Thibaut Sylvestre. "Brillouin light scattering from surface acoustic waves in a subwavelength-diameter optical fibre." *Nature communications* 5, aricle number 5242 (2014).

12 L.D. Landau and E.M. Lifshitz, A.M. Kosevich, L. P. Pitaevskii, Theory of Elasticity (Third edition, Butterworth-Heinemann, Oxford, 1986).

13 Jeffrey L. Bleustein, "A new surface wave in piezoelectric materials." *Applied Physics Letters* 13, no. 12: 412-413(1968).

14 Yu V. Gulyaev, "Electroacoustic surface waves in solids." *ZhETF Pisma Redaktsiiu* 9: 63 (1969) .

15 C. Eckl, A. P. Mayer, and A. S. Kovalev. "Do surface acoustic solitons exist?." *Physical Review Letters* 81, no. 5 (1998): 983.

16 Christophe Taillan, Nicolas Combe, and Joseph Morillo. "Nanoscale self-organization using standing surface acoustic waves." *Physical review letters* 106, no. 7: 076102 (2011).

17 Maurizio Romeo. Surface waves in hexagonal micropolar dielectrics. International Journal of Solids and Structures 87, 39–47 (2016)

18 B.A. Auld, and J. J. Gagnepain. "Horizontal shear surface waves on corrugated surfaces." *Electronics letters* **12** (24), 650 (1976)

19 A. E. H. Love, "Theory of the propagation of seismic waves. Some problems of geodynamics." (1911): 144-178.

20 A. A. Maznev and V. E. Gusev. "Waveguiding by a locally resonant metasurface." *Physical Review **B*** **92** (11), 115422 (2015)

21 Yamada Yasusada, and Gen Shirane. "Neutron scattering and nature of the soft optical phonon in SrTiO3." Journal of the Physical Society of Japan 26, no. 2: 396-403 (1969).

22 G. Shirane and Y. Yamada. Lattice-Dynamical Study of the 110'K Phase Transition in SrTiO3. Physical Review, **177**, (2) 858 (1969).

23 G. Shirane, J. D. Axe, J. Harada, and J. P. Remeika. "Soft ferroelectric modes in lead titanate." *Physical Review* **B 2**, no. 1: 155 (1970)

24 J. D. Axe, J. Harada, and G. Shirane. "Anomalous acoustic dispersion in centrosymmetric crystals with soft optic phonons." *Physical Review B* 1, no. 3: 1227 (1970).

25 R. Currat, H. Buhay, C. H. Perry, and A. M. Quittet. "Inelastic neutron scattering study of anharmonic interactions in orthorhombic KNbO3." *Physical Review* **B 40**, no. 16: 10741 (1989).

26 J. Hlinka, S. Kamba, J. Petzelt, J. Kulda, C. A. Randall, and S. J. Zhang. "Origin of the "Waterfall" effect in phonon dispersion of relaxor perovskites." *Physical review letters* **91**, no. 10 (2003): 107602.

27 W. A. Hamilton, A. G. Klein, G. I. Opat, and P. A. Timmins. "Neutron diffraction by surface acoustic waves." *Physical review letters* 58, no. 26 (1987): 2770.

28 Soffer, B. H., D. H. Close, and M. E. Pedinoff. "An optical imaging method for direct observation and study of acoustic surface waves." *Applied Physics Letters* 15.10 (1969): 339-342.

29 Laura J. Pyrak-Nolte, Jianping Xu, and Guy M. Haley. "Elastic interface waves propagating in a fracture." Physical review letters 68, no. 24 (1992): 3650.

30 M. M. de Lima Jr, Yu A. Kosevich, P. V. Santos, and A. Cantarero. "Surface acoustic bloch oscillations, the wannier-stark ladder, and landau-zener tunneling in a solid." *Physical review letters* 104, no. 16 (2010): 165502.

31 A. Kohutych, R. Yevych, S. Perechinskii, V. Samulionis, J. Banys, and Yu Vysochanskii. Sound behavior near the Lifshitz point in proper ferroelectrics. Physical Review **B 82**, no. 5: 054101 (2010).

32 K. Z. Rushchanskii, A. Molnar, R. Bilanych, R. Yevych, A. Kohutych, and Yu. M. Vysochanskii, V. Samulionis and J. Banys. "Observation of nonequilibrium behavior near the Lifshitz point in ferroelectrics with incommensurate phase". Phys.Rev. **B 93**, 014101 (2016)

33 J. Hlinka, I. Gregora, and V. Vorlıcek. Complete spectrum of long-wavelength phonon modes in Sn2P2S6 by Raman scattering. Phys.Rev. **B 65**, 064308 (2002)

34 J. Hlinka, I. Gregora, and V. Vorlıcek. Complete spectrum of long-wavelength phonon modes in Sn2P2S6 by Raman scattering. Phys.Rev. **B 65**, 064308 (2002)

35 G. Dovbeshko, O Fesenko, A Dementjev , R Karpicz , V Fedorov , OY Posudievsky. Coherent anti-Stokes Raman scattering enhancement of thymine adsorbed on graphene oxide. Nanoscale Res Lett., **9**(1):26B (2014)

36 Yl. Sugawara, O. B. Wright, O. Matsuda, M. Takigahira, Yl Tanaka, S. Tamura, and V. E. Gusev. "Watching ripples on crystals." *Phys. Rev. Lett.* **88** (18), 185504 (2002)

37 Kimmo Kokkonen, Matti Kaivola, Sarah Benchabane, Abdelkrim Khelif, and V. Laude. "Scattering of surface acoustic waves by a phononic crystal revealed by heterodyne interferometry." *Appl. Phys. Lett.* **91**(8), 083517 (2007)

38 P. Mutti, C. E. Bottani, G. Ghislotti, M. Beghi, G. A. D. Briggs, and J. R. Sandercock. "Surface Brillouin scattering—Extending surface wave measurements to 20 GHz." Chapter 7 (p. 249-300) in "Advances in acoustic microscopy" (1995).

39 A. G. Every, L. M. Kotane, and J. D. Comins. "Characteristic wave speeds in the surface Brillouin scattering measurement of elastic constants of crystals." Physical Review **B 81** (22), 224303 (2010).

40 V. S. Mashkevich and K. B. Tolpygo, "The interaction of vibrations of nonpolar crystals with electric fields." Zh. Eksp. Teor. Fiz. **31**, 520 (1957).

41 Sh. M. Kogan. Piezoelectric effect under an inhomogeneous strain and an acoustic scattering of carriers of current in crystals Solid State Physics, Vol. **5**, 10, 2829 (1963)

42 A.K. Tagantsev, Piezoelectricity and flexoelectricity in crystalline dielectrics. Phys. Rev B, **34**, 5883 (1986)

43 P V Yudin and A K Tagantsev. Fundamentals of flexoelectricity in solids. Nanotechnology, **24**, 432001 (2013);

44 J. Narvaez and G. Catalan, Origin of the enhanced flexoelectricity of relaxor ferroelectrics, Applied Physics Letters **104**, 162903 (2014)

45 P. Zubko, G. Catalan, A.K. Tagantsev. Flexoelectric Effect in Solids. Annual Review of Materials Research 43: 387-421. (2013).

46 A. Kvasov, and A. K. Tagantsev. "Dynamic flexoelectric effect in perovskites from first-principles calculations." *Physical Review B* 92, 054104 (2015).

47 Anna N. Morozovska, Yulian M. Vysochanskii, Oleksandr V. Varenyk, Maxim V. Silibin, Sergei V. Kalinin, and Eugene A. Eliseev. "Flexocoupling impact on the generalized susceptibility and soft phonon modes in the ordered phase of ferroics". *Physical Review* B 92, 094308 (2015).

48 Anna N. Morozovska, Eugene A. Eliseev, Christian M. Scherbakov, and Yulian M. Vysochanskii, The influence of elastic strain gradient on the upper limit of flexocoupling strength, spatially-modulated phases and soft phonon dispersion in ferroics. *Phys. Rev.* B 94, 174112 (2016)

49 "Flexoelectricity in Solids: From Theory to Applications". Ed. by A.K. Tagantsev and P.V. Yudin, World Scientific (2016).

50 J.H.Barrett, Dielectric Constant in Perovskite Type Crystals. Physical Review, vol. 86, Issue 1, pp. 118-120 (1952).

51 E.A. Eliseev, A.N. Morozovska, M.D. Glinchuk, and R. Blinc. Spontaneous flexoelectric/flexomagnetic effect in nanoferroics. Phys. Rev. B. 79, № 16, 165433-1-10, (2009).

52 P. V. Yudin, R. Ahluwalia, A. K. Tagantsev. Upper bounds for flexocoupling coefficients in ferroelectrics, Appl.Phys.Lett. **104**(8), 082913 (2014)

53 See Supplemental Material at [URL will be provided by Publisher] for the derivation of the Euler-Lagrange equations

54 Y. L. Li, S. Choudhury, J. H. Haeni, M. D. Biegalski, A. Vasudevarao, A. Sharan, H. Z. Ma, J.Levy, V.Gopalan, S. Trolier-McKinstry, and D.G. Schlom. "Phase transitions and domain structures in strained pseudocubic (100) $SrTiO_3$ thin films." *Physical Review B* 73, no. 18: 184112 (2006).

55 A.K. Tagantsev, E. Courtens and L. Arzel. "Prediction of a low-temperature ferroelectric instability in antiphase domain boundaries of strontium titanate." Phys. Rev. B, **64**, 224107 (2001).

56. P.A. Fleury and J. M. Worlock. "Electric-Field-Induced Raman Scattering in SrTi O 3 and KTa O 3." Phys. Rev. **174**, 613 (1968).

57 N. A. Pertsev, A. K. Tagantsev, and N. Setter. "Phase transitions and strain-induced ferroelectricity in SrTiO 3 epitaxial thin films." Phys. Rev. B **61**, R825 (2000).

58 P. Zubko, G. Catalan, A. Buckley, P. R. L. Welche, and J. F. Scott. "Erratum: Strain-Gradient-Induced Polarization in SrTiO 3 Single Crystals [Phys. Rev. Lett. 99, 167601 (2007)]." *Physical Review Letters* 100, no. 19 (2008): 199906.

59 P. Zubko, G. Catalan, A. Buckley, P. R. L. Welche, and J. F. Scott, Phys. Rev. Lett. **99**, 167601 (2007).

60 Alberto Biancoli, Chris M. Fancher, Jacob L. Jones, and Dragan Damjanovic. "Breaking of macroscopic centric symmetry in paraelectric phases of ferroelectric materials and implications for flexoelectricity." *Nature materials* 14, no. 2 (2015): 224-229.

61 M. Stengel, "Unified ab initio formulation of flexoelectricity and strain-gradient elasticity." *Physical Review* **B 93**, no. 24 (2016): 245107.

62 M. Stengel, Flexoelectricity from density-functional perturbation theory, Phys. Rev. B **88**, 174106 (2013).